Effective One Step-iterative Fiducial Marker-based Compensation for Involuntary Motion in Weight-bearing C-arm Cone-beam CT Scanning of Knees

Jang-Hwan Choi[1,2], Andreas Maier[3], Martin Berger[3,4], Rebecca Fahrig[1]

[1] Department of Radiology, Stanford University, Stanford, CA 94305;
[2] Department of Mechanical Engineering, Stanford University, Stanford, CA 94305;
[3] Friedrich-Alexander University Erlangen-Nuremberg, 91058 Erlangen, Germany;
[4] Graduate School Heterogeneous Image Systems, FAU Erlangen-Nuremberg, Germany;

ABSTRACT

We previously introduced three different fiducial marker-based correction methods (2D projection shifting, 2D projection warping, and 3D image warping) for patients' involuntary motion in the lower body during weight-bearing C-arm CT scanning. The 3D warping method performed better than 2D methods since it could more accurately take into account the lower body motion in 3D.

However, as the 3D warping method applies different rotational and translational movement to the reconstructed image for each projection frame, distance-related weightings were slightly twisted and thus result in overlaying background noise over the entire image. In order to suppress background noise and artifacts (e.g. metallic marker-caused streaks), the 3D warping method has been improved by incorporating bilateral filtering and a Landweber-type iteration in one step.

A series of projection images of five healthy volunteers standing at various flexion angles were acquired using a C-arm cone-beam CT system with a flat panel. A horizontal scanning trajectory of the C-arm was calibrated to generate projection matrices. Using the projection matrices, the static reference marker coordinates in 3D were estimated and used for the improved 3D warping method.

The improved 3D warping method effectively reduced background noise down below the noise level of 2D methods and also eliminated metal-generated streaks. Thus, improved visibility of soft tissue structures (e.g. fat and muscle) was achieved while maintaining sharp edges at bone-tissue interfaces. Any high resolution weight-bearing cone-beam CT system can apply this method for motion compensation.

Keywords: weight-bearing knee, C-arm cone-beam CT, Landweber type iteration, bilateral filtering, motion artifacts, fiducial marker, medical image processing

1. INTRODUCTION

Imaging patients *in vivo* under non-weight-bearing might lead to altered diagnoses regarding knee cartilage health since knee joint kinematics in supine or prone positions have been shown to be different from those under weight-

bearing conditions[1-3]. A C-arm cone-beam CT system has flexible imaging trajectories as well as wide volumetric beam coverage which enable the system to image both knees together under weight-bearing conditions[4-6].

However, standing subjects have more involuntary motion than patients lying on a table and thus reconstructed images acquired under weight-bearing conditions are particularly susceptible to severe motion artifacts. Our previous study proposed the use of fiducial markers for three different correction methods in two dimensions (2D) or three dimensions (3D) for involuntary motion compensation[5]. The three methods (2D projection shifting, 2D projection warping, and 3D image warping) effective in improving quantitative and qualitative image quality . The 3D image warping method performed best and showed the largest increase in the Structural SIMilarity (SSIM) index since 2D methods cannot accurately incorporate fiducial marker locations in 3D along the x-ray path[5].

The 3D image warping method is still limited as it warps 3D images for each projection image during the process of reconstruction, which violates the assumption of the filtered back-projection algorithm that a subject is immobile during the scanning. This patient motion combined with our correction approach caused distortion of distance-related weightings and resulted in low-frequency background noise over the entire image and higher overall CT number compared to the 2D methods. In this study, we propose a simple but effective improved 3D warping method incorporating one step of a Landweber type iteration [7] and bilateral filtering [8] to remove this artifact.

2. MATERIALS AND METHODS

2.1 Experimental setup

A C-arm cone-beam CT system (Axiom Artis dTA, Siemens AG, Forchheim, Germany) with a flat panel detector was used to image five healthy volunteers while standing in an upright position and squatting at different knee flexion angles. The acquisition protocol consisted of 70 kVp tube voltage request, 1.2 μGy/frame detector dose request, and 248 frames over π plus fan angle in 10 seconds. Each individual projection has 1240×960 pixels with 0.308 mm isotropic resolution after 2×2 binning. A total of nine tantalum spherical markers with 1mm diameter were carefully attached around both knees. A geometrical calibration for the weight-bearing C-arm trajectory (i.e. a C-arm rotates in a horizontal trajectory) was achieved using the PDS-2 phantom which generated 248 projection matrices[6].

2.2 Estimation of the static reference marker coordinates in 3D

The static reference marker $\vec{x}$ (i.e. 3D reference) coordinates $(\bar{x}, \bar{y}, \bar{z})$ of each marker were estimated by back-projecting the marker in 2D multiple projection images using the acquired projection matrices as follows. First, a projection matrix linked an individual voxel in 3D to the 2D point in every projection image as shown in Eq. (1).

$$\mathbf{P_j} \cdot \begin{pmatrix} \bar{x} \\ \bar{y} \\ \bar{z} \\ 1 \end{pmatrix} = \begin{bmatrix} \bar{p}_{j,1}^{T} & p_{j,14} \\ \bar{p}_{j,2}^{T} & p_{j,24} \\ \bar{p}_{j,3}^{T} & p_{j,34} \end{bmatrix} \cdot \begin{pmatrix} \bar{x} \\ \bar{y} \\ \bar{z} \\ 1 \end{pmatrix} = \begin{pmatrix} u_j \\ v_j \\ 1 \end{pmatrix} \cdot \xi_j, \tag{1}$$

where (u_j, v_j) indicates a marker's 2D coordinates in the j^{th} projection image, $p_{j,mn}$ is the element in m^{th} row and n^{th} column of the j^{th} projection matrix (P_j), ξ_j is a homogeneous term, and $\bar{p}_{j,m}^{T} = (p_{j,m1} \quad p_{j,m2} \quad p_{j,m3})$ [9]. Several rearrangements lead to Eq. (2) below. The complete derivation can be found in Choi et al[9].

$$\operatorname{argmin}_{\vec{x}} \left\| \begin{bmatrix} u_1 \cdot \vec{p}_{1,3}^{T} - \vec{p}_{1,1}^{T} \\ v_1 \cdot \vec{p}_{1,3}^{T} - \vec{p}_{1,2}^{T} \\ u_2 \cdot \vec{p}_{2,3}^{T} - \vec{p}_{2,1}^{T} \\ v_2 \cdot \vec{p}_{2,3}^{T} - \vec{p}_{2,2}^{T} \\ \vdots \\ u_N \cdot \vec{p}_{N,3}^{T} - \vec{p}_{N,1}^{T} \\ v_N \cdot \vec{p}_{N,3}^{T} - \vec{p}_{N,2}^{T} \end{bmatrix} \cdot \vec{x} - \begin{pmatrix} -u_1 \cdot p_{1,34} + p_{1,14} \\ -v_1 \cdot p_{1,34} + p_{1,24} \\ -u_2 \cdot p_{2,34} + p_{2,14} \\ -v_2 \cdot p_{2,34} + p_{2,24} \\ \vdots \\ -u_N \cdot p_{N,34} + p_{N,14} \\ -v_N \cdot p_{N,34} + p_{N,24} \end{pmatrix} \right\|_2^2, \quad (2)$$

where N (248) is the number of projections. The objective function in Eq. (2) basically finds a point that fits the projected points best. Hereafter, the 3D reference's forward-projected point in the 2D projection is called the 2D reference ($\vec{r}'_{i,j} = P_j \cdot (\bar{x}, \bar{y}, \bar{z})$).

2.3 Improved 3D warping motion correction method (i.e. iterative 3D warping)

The previous 3D warping method found an optimal rotation matrix R_j and translation matrix T_j for a volumetric image in the j^{th} projection minimizing the Euclidean distance from the i^{th} marker ($\vec{m}_{i,j}$) to the R_j-and T_j-transformed 2D reference ($\vec{r}'_{i,j}$).[5] The optimization problem is found as described in Eq. (3) below.

$$\operatorname{argmin}_{R_j,T_j} \sum_i \left\| \vec{r}'_{i,j} - \vec{m}_{i,j} \right\|^2. \quad (3)$$

Embedding of the motion into the back-projection was performed as described in D. Schaefer et al. (2006)[10]. Graphics hardware (GPU) [11] accelerated-reconstruction was performed using our software framework (CONRAD) [12] to generate 512×512×512 voxels with 0.5 mm isotropic spacing. The reconstruction was performed with a modified Shepp-Logan ramp filter with roll-off [13] for a smooth cutoff at high frequencies.

Then, a bilateral filter was applied to image voxel vector x^0 of the initial motion-corrected reconstruction. A bilateral filter decides a weight for the individual voxel vector based on spatial distance (σ_s) as well as the radiometric differences (σ_r) which enables the smoothing of noise only if the noise level is below the minimum amplitude of an edge (σ_r) that we want to preserve. Note that following a normal Gaussian distribution, there will be still about 68 % smoothing at an edge of σ_r. In this study, σ_r is set based on the intensity difference between fat and muscle. Finally, we initialized a Landweber-type reconstruction in one step using the FDK algorithm[7, 14]. Note that this combination of bilateral filtering and Landweber iterations is an approximation of a TV-regularized iterative reconstruction[15]. These processing steps are described in order below.

i. Acquire initial motion-corrected reconstruction (x^0) using the 3D warping method and Eq. (3)
ii. Apply a 3D bilateral filter on voxel vector x^0 with σ_s and σ_r
iii. One step Landweber-type reconstruction using the FDK algorithm: $x^1 = x^0 + \lambda A^T(b - Ax^0)$, where A is a forward-projector, A^T is a backward-projector, λ is a step size, and b is projected data in 2D.

In the step (iii) above, λ was determined heuristically as 0.5. The computed motion (R_j and T_j) was embedded in A and A^T.

2.4 Measurement of noise reduction and the line profile

In order to assess the image quality of the resulting images (x^1) compared to the initial motion-corrected reconstruction (x^0), we measured noise level (% standard deviation) over the air region between legs as indicated by the arrow in Figure 1 (c3). We also measured the two line profiles across the edge between fat and muscle, and the edge between cortical bone and fat which represent an edge with a low contrast and an edge with high contrast, respectively.

3. RESULTS

Figure 1 shows representative reconstructed slices of the subject with the largest involuntary motion among five healthy volunteers. In order to compare noise level, motion correction using the 2D simple shifting (refer to Choi et al.[5]) was also applied. As the arrows in (a3) and (b3) indicate, tantalum markers induced fan-shaped radial streaks which degraded soft tissue visibility. The iterative 3D warping in the rightmost column almost completely suppressed the streak artifacts. The arrows in (c3) point to the areas where severe low-frequency background noise is present. The iterative 3D warping successfully decreased the background noise over the entire image. Noise levels for (c1 to c4) were 33.3, 12.2, 11.7, and 9.5 %, respectively. As expected from the edge-preserving property of a bilateral filter, edges over the threshold level (σ_r) were well preserved. Because of the reduction of noise and artifacts, the iterative 3D warping improved image quality compared to the previous 3D warping.

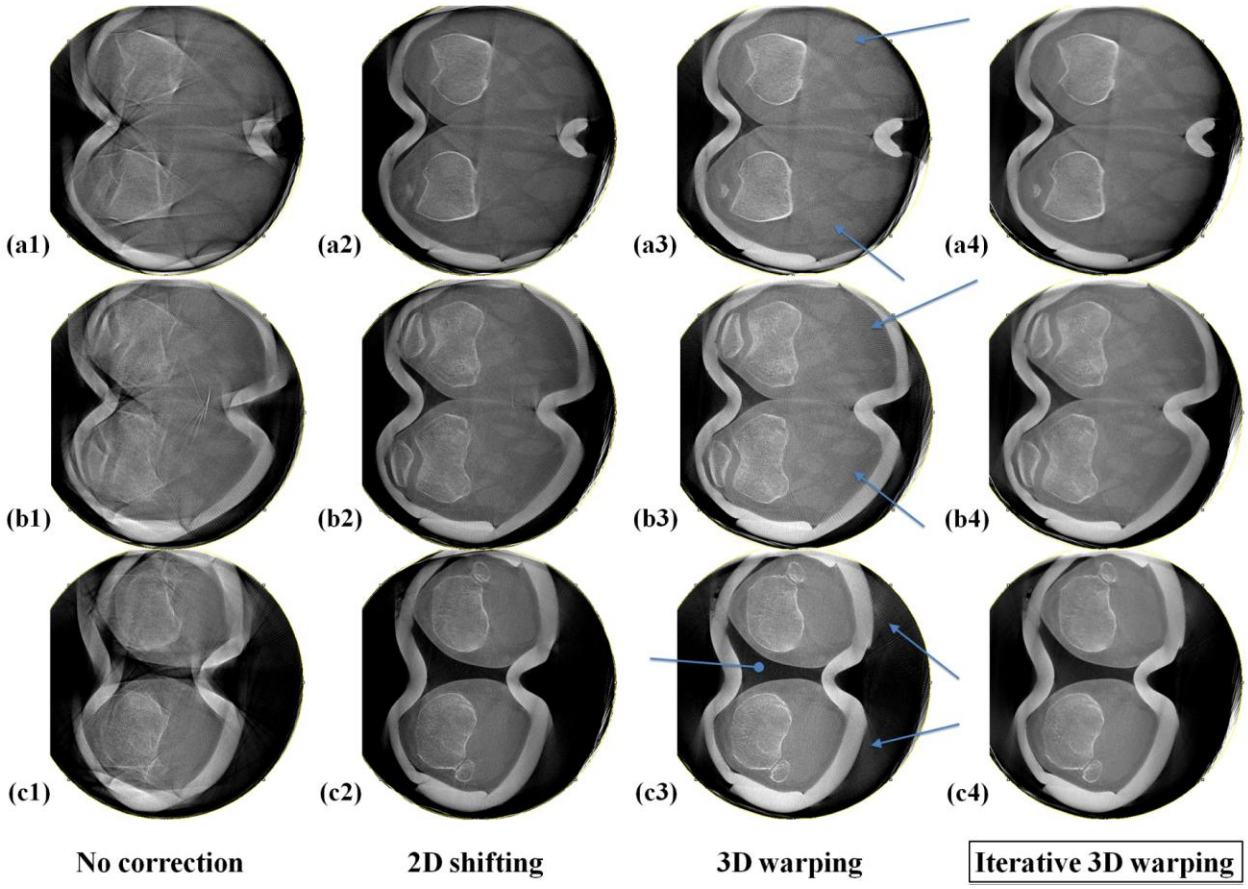

Figure 1. Representative reconstructed slices of a healthy volunteer squatting at a 35˚ knee flexion angle. The first row (a1 to a4), the second row (b1 to b4), and the third row (c1 to c4) show upper off-center, central, and lower off-center axial slices. The rightmost column contains slices corrected using our newly proposed iterative 3D warping method.

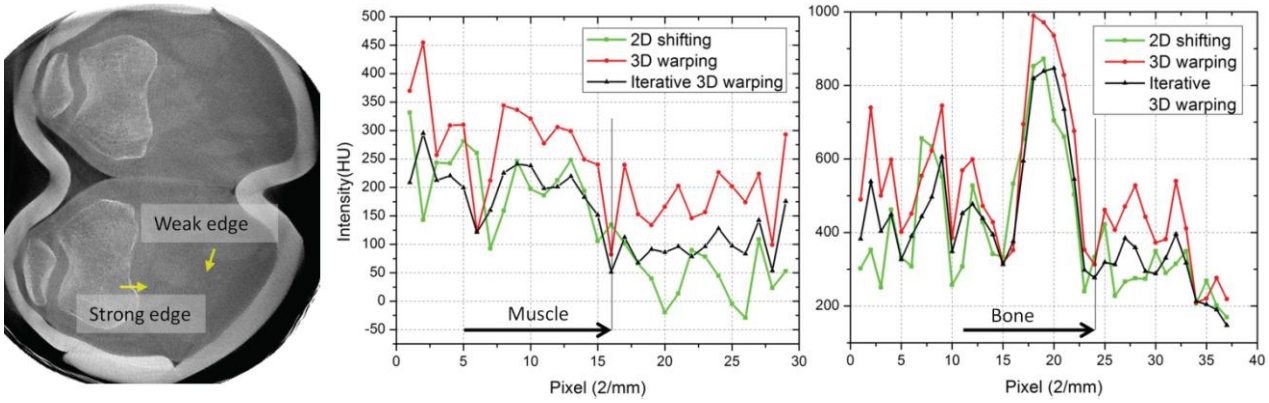

(a) Region of interest (ROI) for line profiles in (b) and (c)

(b) Line profiles over the weak edge in (a)

(c) Line profiles over the strong edge in (a)

Figure 2. Three correction methods' representative line profiles over the weak edge and strong edge as drawn with arrows in (a). (a) The ROIs for the line profiles were in the central slice. (b) The line profiles of the weak edge were drawn across muscle and fat. (c) The line profiles of the strong edge were drawn across bone and fat.

Figure 2 shows the line profiles of the weak edge (muscle-fat) and strong edge (bone-fat). The line profiles were acquired from the same subject data as in Figure 1. As observed qualitatively in Figure 1, the line profiles of the weak edge confirmed that edges with low contrast were well preserved without serious degradation of spatial resolution. The iterative 3D warping made both the weak edge and strong edge more distinctive by suppressing noise and artifacts in the low density material (fat). For instance, compared with the 3D warping, the iterative 3D warping increased the intensity differences between the high density material and the low density material represented by the amplitude of the first peaks on the left- and right-side of the black vertical line, respectively, shown in Figure 2 (b) and (c). One step Landweber-type iteration with λ of 0.5 ($x^1 = x^0 + \lambda A^T(b - Ax^0)$) decreased the overall CT number so that it was close to the intensity level of the 2D shift-corrected reconstruction.

4. CONCLUSIONS

Although the previous 3D warping method performed better than 2D methods, the method suffered from underlying noise due to distance-related weighting distortion. We developed a simple but effective improved 3D warping method incorporating one step of a Landweber type iteration and bilateral filtering. The newly proposed improved 3D warping method (i.e. iterative 3D warping) suppressed background noise effectively and also reduced artifacts such as metal marker-induced streaks while preserving fine spatial resolution. The noise level in the representative slice with iterative 3D warping was lower by at least 2.2 % than that with other methods.

ACKNOWLEDGEMENT

The authors would like to thank Saikat Pal, Garry Gold, and Emily J. McWalter for their tremendous help with acquisition of a experimental data and Gary Beaupre for his insightful advice on experimental setup. This work was supported by NIH 1 R01HL087917, Siemens Medical Solutions, the Lucas Foundation, CBIS (Center for Biomedical Imaging at Stanford) Seed Funding and the Research Training Group 1773 "Heterogeneous Image Systems", funded by the German Research Foundation (DFG). This work was never submitted, published, or presented before.

REFERENCES

[1] Draper, C. E., Besier, T. F., Fredericson, M., Santos, J. M., Beaupre, G. S., Delp, S. L. and Gold, G. E., "Differences in patellofemoral kinematics between weight-bearing and non-weight-bearing conditions in patients with patellofemoral pain," Journal of orthopaedic research : official publication of the Orthopaedic Research Society, 29(3), 312-7 (2011).

[2] Powers, C. M., Ward, S. R., Fredericson, M., Guillet, M. and Shellock, F. G., "Patellofemoral kinematics during weight-bearing and non-weight-bearing knee extension in persons with lateral subluxation of the patella: a preliminary study," The Journal of orthopaedic and sports physical therapy, 33(11), 677-85 (2003).

[3] Choi, J.-H., McWalter, E. J., Pal, S., Maier, A., Gold, G. E. and Fahrig, R., "Analysis of Three-dimensional Joint Space of the Tibiofemoral Joint," in Nuclear Science Symposium and Medical Imaging Conference (NSS/MIC), Seoul, Korea, (2013).

[4] Choi, J. H., Keil, A., Maier, A., Pal, S., McWalter, E. J. and Fahrig, R., "Fiducial Marker-Based Motion Compensation for the Acquisition of 3D Knee Geometry Under Weight-Bearing Conditions Using a C-Arm CT Scanner," in AAPM 54th Annual Meeting, Charlotte, NC, (2012), pp. 3973-3973.

[5] Choi, J.-H., Fahrig, R., Keil, A., Besier, T. F., Pal, S., McWalter, E. J., Beaupré, G. S. and Maier, A., "Fiducial marker-based correction for involuntary motion in weight-bearing C-arm CT scanning of knees. Part I. Numerical model-based optimization," Med Phys, 40(9), 091905 (2013).

[6] Maier, A., Choi, J.-H., Keil, A., Niebler, C., Sarmiento, M., Fieselmann, A., Gold, G., Delp, S. and Fahrig, R., "Analysis of vertical and horizontal circular C-arm trajectories," in Proc SPIE, Lake Buena Vista, Florida, (2011), pp. 796123-8.

[7] Landweber, L., "An iteration formula for Fredholm integral equations of the first kind with application to the axially symmetric potential flow about elongated bodies of revolution," Thesis - University of Maryland, College Park., 1951.

[8] Tomasi, C. and Manduchi, R., "Bilateral filtering for gray and color images," Sixth International Conference on Computer Vision, 839-846 (1998).

[9] Choi, J.-H., Maier, A., Keil, A., Pal, S., McWalter, E. J., Beaupré, G. S., Gold, G. E. and Fahrig, R., "Fiducial Marker-based Correction for Involuntary Motion in Weight-bearing C-arm CT Scanning of Knees. Part II. Experiment," Med Phys (under review), (2013).

[10] Schafer, D., Borgert, J., Rasche, V. and Grass, M., "Motion-compensated and gated cone beam filtered back-projection for 3-D rotational X-ray angiography," IEEE Trans Med Imaging, 25(7), 898-906 (2006).

[11] Scherl, H., Keck, B., Kowarschik, M. and Hornegger, J., "Fast GPU-based CT reconstruction using the common unified device architecture (CUDA)," in IEEE Nucl Sci Conf R, (2007), pp. 4464-4466.

[12] Maier, A., Hofmann, H. G., Berger, M., Fischer, P., Schwemmer, C., Wu, H., Muller, K., Hornegger, J., Choi, J. H., Riess, C., Keil, A. and Fahrig, R., "CONRAD-A software framework for cone-beam imaging in radiology," Med Phys, 40(11), 111914 (2013).

[13] Kak, A. C. and Slaney, M., [Principles of computerized tomographic imaging], Society for Industrial and Applied Mathematics, Philadelphia (2001).

[14] Feldkamp, L. A., Davis, L. C. and Kress, J. W., "Practical Cone-Beam Algorithm," Journal of the Optical Society of America a-Optics Image Science and Vision, 1(6), 612-619 (1984).

[15] Manhart, M. T., Kowarschik, M., Fieselmann, A., Deuerling-Zheng, Y., Royalty, K., Maier, A. K. and Hornegger, J., "Dynamic Iterative Reconstruction for Interventional 4-D C-Arm CT Perfusion Imaging," IEEE Trans Med Imaging, 32(7), 1336-48 (2013).